Hindawi Publishing Corporation
Modelling and Simulation in Engineering
Volume 2015, Article ID 729582, 11 pages
http://dx.doi.org/10.1155/2015/729582

Research Article

Characterization and Modelling of LeBlanc Hydrodynamic Stabilizer: A Novel Approach for Steady and Transient State Models

Marlon Wesley Machado Cunico

Department of Mechanical Engineering, University of São Paulo, 80320-260 São Carlos, PR, Brazil

Correspondence should be addressed to Marlon Wesley Machado Cunico; marloncunico@yahoo.com.br

Received 14 October 2014; Revised 12 March 2015; Accepted 14 March 2015

Academic Editor: Aiguo Song

As result of increase of customers' demands, products become more complexes and dynamics control increased its role into product development. As example, clothing washing machines use LeBlanc balancers in order to reduce vibration issues. Nevertheless, the behaviour of such apparatus is still hard to describe and the numerical simulation of this sort of vibration control is based on ball rings. The main goal of this work is to define and characterize a numerical model that describes the hydrodynamics balance ring in the transient state in addition to steady state models. As consequence, the behaviour of balance ring was identified in a computational fluid dynamics tool and an equation that describes restoration forces, unbalance, force phase, and eccentricity was found.

1. Introduction

Along the last years, the demand for high performance appliances has been growing progressively, making the development of vertical axis washing machines be guided by either the increase of capacity, water extraction, washing quality, reduction of vibration or noise. As a consequence of increase of capacity, the gaps between components such as cabinet and tub tend to be decreased, while the increase of basket rotation intends to improve water extraction. Therefore, this combination of factors tends to create more severe application conditions, where the isolator and stabilizer systems are essential to ensure the machine design.

One of the most common stabilizer systems which are possible to be found in vertical axis washing machines is the LeBlanc stabilizer, which is also known as hydrodynamic balance ring, as shown in Figure 1. In this figure, the main elements of a vertical washing machine are also presented, where an unbalance mass represents the unbalance which is caused by clothes during agitation and water extraction [1, 2].

This LeBlanc stabilizer consists in the hollow ring which is partially filled by fluid and has the reduction of vibration in the water extraction stage (spinning) as its main purpose. In the spinning stage, it is common that the clothes are implied on unbalance mass, which induce vibration of washing system and generate forces in the basket. Among the main consequences of this condition, we can highlight the contact between basket and tub, the contact between tub and cabinet, and the excessive vibration of machine, which can even result in walking machine [1–8].

In spite of the high volume of researches related to balance ring and washing machine dynamics, most of the models which are found in these studies ignore the transient response and still have several challenges to be overcome. In addition, the computational implementation of these models in dynamic system is very difficult and hardly results in a confident transient response [4]. As alternative to such complexity, the balance ring model which is the most used in dynamic studies consists in distribution of balls inside a ring where the friction provides dampening of ball motion [2–6, 8].

For that reason, the main goal of this work is to propose a novel model of balance ring which considers either steady or transient state, being easily implemented in a computational

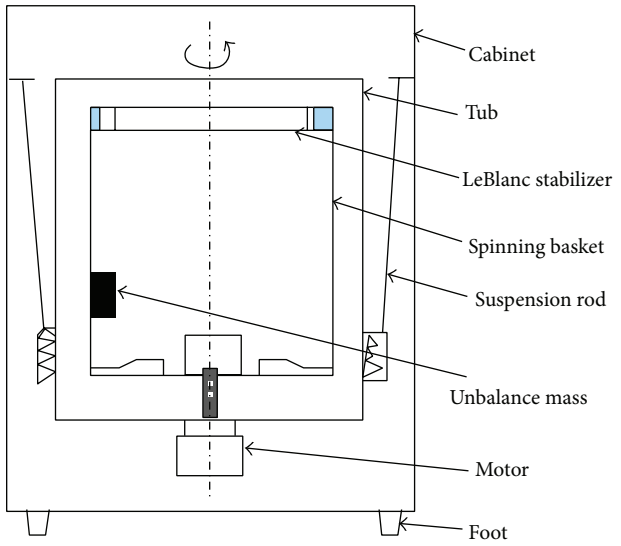

Figure 1: Schematic of a vertical axis washing machine and their main components.

dynamical system. In addition, the model was implemented in dynamic system in the plane, evidencing the benefits of balance ring to the washing machine. To achieve this purpose, this work was divided into 3 parts, steady state, transient state, and dynamical system implementation.

For the steady state study, we applied response surface method to identify the behaviour of balance ring as a function of eccentricity, orbit direction, and rotation rate. The responses of this study are balance ring force (restoration or counterbalance force) and water distribution (unbalance water mass inside chamber).

Another point in this study is the decomposing of eccentricity, orbit direction, and rotation in the translational and rotational movement increment along the time. Therefore, it allows us to identify the instantaneous restoration force and force angle phase with respect to unbalance load.

For the transient analysis, we submitted the balance ring to 4 different change states levels at the same rotation, analysing the behaviour of restoration force and water distribution between these states. In this way, a transition equation which defines the behaviour of balance ring in either steady or transient states was identified.

At the end, we applied this model in a simplified dynamical model in order to identify the contribution of balance ring to the dynamics and main efforts of machine.

2. Material and Methods

For the steady state study, we applied a response surface with 3 variables and 5 levels. Where eccentricity, orbit orientation, and rotation speed are the control factors and restoration force, restoration force angle and water distribution are the responses. These responses were acquired through a computational fluid dynamics (CFD) analysis, where a multiphase method has been used to model the behaviour of fluid inside the ring chamber.

Table 1: Response surface design matrix.

Variables	Control factor levels				
	−2	−1	0	+1	+2
Eccentricity (mm)	1	4,5	8	11,5	15
Rotation speed (rpm)	50	225	400	575	750
Orbit orientation	0°		45°		90

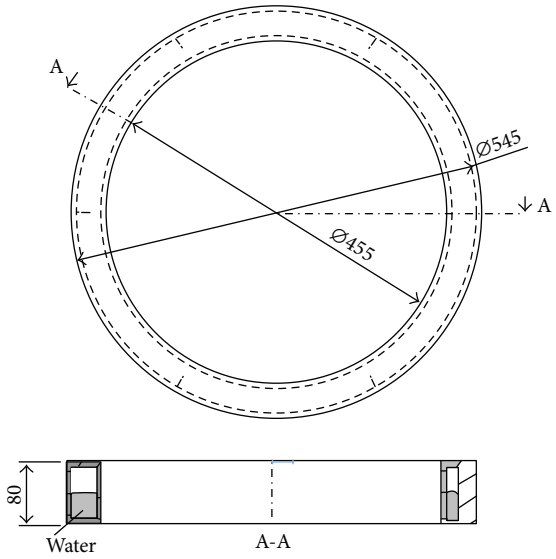

Figure 2: Schematic of simplified LeBlanc stabilizer.

For this study, we also considered the LeBlanc stabilizer with 50% of internal volume filled with water and its geometry are constants. At this point, the main geometrical characteristics of this ring are 455 mm of inner diameter; 545 mm of outer diameter; 80 mm of height; and 6 thins with 80 mm of height and 20 mm of length. A schematic of this geometry can be seen in Figure 2.

In Table 1, it is possible to see the study design matrix, where the values variables in each one of their 5 levels are presented. The eccentricity values vary from 1 to 15 mm, rotation speed varies from 50 to 850 rpm, and orbit orientation varies from 0 to 90°.

For the simulation model, we defined the average mesh size equal to 0.1 mm and 8 prism exponential layers. For the transient multiphase domain, we applied volume of fluid (VOF) method where air and water were the fluids phases. We also used for the transient state study a time step equal to 0.00001 seconds and an error of 10^{-8} per interaction. In addition, the CFD software that was used to simulate this experimental study was STAR CCM+.

With respect to the orbit orientation, it refers to the way the eccentricity is promoted. For analysing this situation, we assumed that the balance ring has a local and movable coordinate system which is placed in the centre of the ring. As a consequence, we defined the eccentricity and orbit orientation through the combination of rotation and translation motion as presented in (4) and (5).

Table 2: Design matrix of level change.

Eccentricity 1	Eccentricity 2	Change level	Time (s)	Transient equation
10 mm	1	−9 mm	1,5	$F = 400 - (300 - 300 \cdot e^{-3 \cdot t})$
10 mm	5 mm	−5 mm	1,5	$F = 400 - (150 - 150 \cdot e^{-3 \cdot t})$
1 mm	10 mm	9 mm	1,5	$F = 100 + (300 - 300 \cdot e^{-3 \cdot t})$
5 mm	10 mm	4 mm	1,5	$F = 250 + (150 - 150 \cdot e^{-3 \cdot t})$

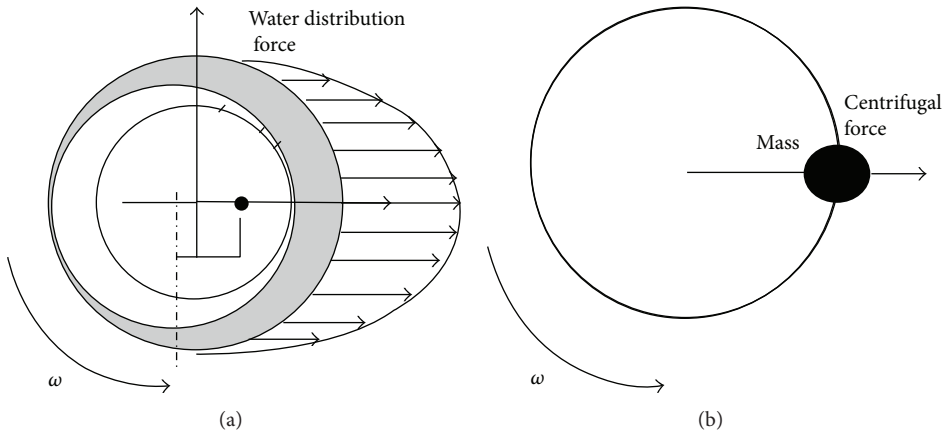

Figure 3: Schematic of restoration force simplification from distributed water force (a) and single mass centrifugal force (b).

For analysis of study responses, we included a reference unbalance load which is useful to determine the phase angle between restoration and unbalance forces. It was also assumed that the restoration force might be represented by just a single mass centrifugal force, simplifying the force which resulted from water distribution, as presented in Figure 3.

For the transient analysis, we analysed the behaviour of restoration force, restoration force angle, and time needed to change between states, as shown in Figure 4. In this figure, it is possible to see the change of states level, such as the transition area, 3 types of transition behaviour, and the definition of each state.

In this case, we selected 4 changes of states levels where the eccentricity varied from 10 to 1 mm, 10 to 5 mm, 1 to 10 mm, and 5 to 10 mm. In Table 2 a matrix with values of eccentricity that define the states and the change of states level is presented. In addition, this table also shows the value of transient time (t_1–t_0) and a fitted curve equation which might define the transient state as a function of time.

At the end, we built a rigid body model with 3 degrees of freedom which concerns the proposal balance ring model, the spring stiffness, and viscous damping (friction) in x and y. In addition, the washing group mass and unbalance force are also considered in this model. In Figure 5, it is possible to see a schematic of this model, where an unbalance load provides an excitation to the system which is initially stopped. In addition, this figure also presents the main parameters of this system, such as stiffness, friction, mass, and unbalance load.

In order to analyse the influence of LeBlanc stabilizer on this system in different conditions, we forced 3 specific

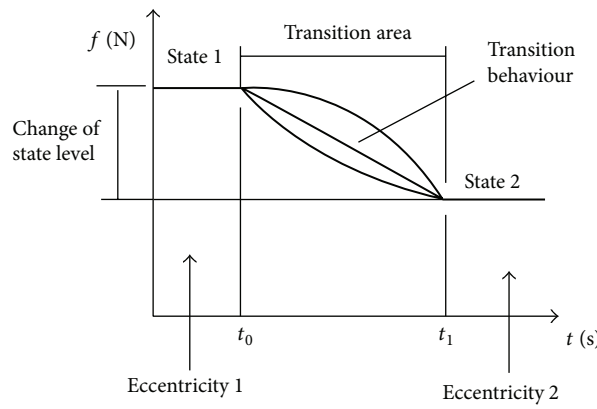

Figure 4: Schematic of transition between states.

rotation speed ramps (15, 20, and 25 rpm/s), as shown in Figure 6. As a result, we analyzed the force of ring, force of unbalance load, and generated orbit. It is important to note that these rotational speed ramps were selected in order to identify the effect of acceleration in LeBlanc stabilizers. In addition, as these values are commonly used in washing machines, the results of this work might be directly applied to optimize such machines.

3. Results and Discussions

In the steady state study, it was possible to identify the variation of ring force, the simplified mass distribution, and angle phase between unbalance load (reference) and restoration force. The results that were acquired from CFD

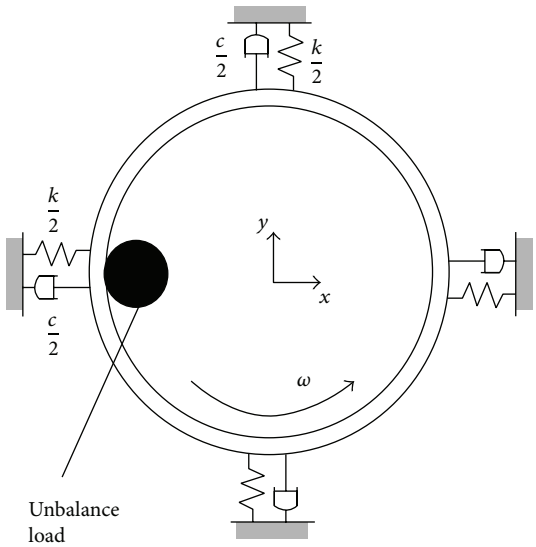

$k = 600\,\text{N/m}$
$c = 1\,\text{N·s/m}$
Mass = 6 kg
Unbalance load = 0.5 kg

Figure 5: Schematic of 3 degrees of freedom (DoF) model.

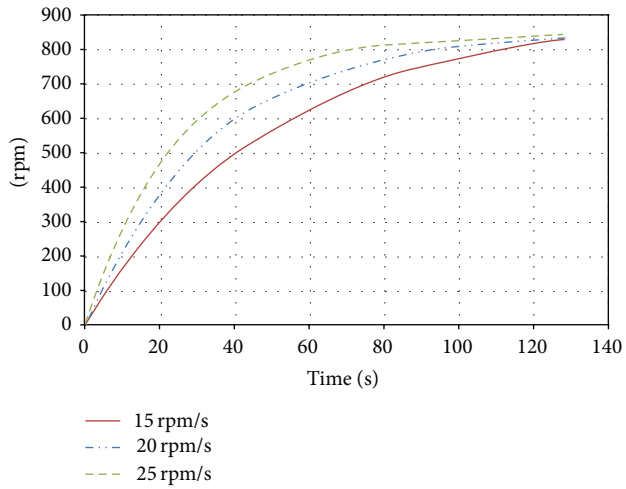

Figure 6: Diagram of rotation speed ramps.

analysis were presented in Table 3, where either the control factors or the response factors are presented.

In Table 3, a reference unbalance load force which results from 0.3 kg of unbalance can also be seen. Through this reference, it is possible to identify the effectiveness of balance ring restoration force, whereas the equilibrium between these forces might indicate the steady state orbit of system. For example, if the orbit orientation was 180°, the rotation was 400 rpm, and the unbalance load was 0.3 kg, the restoration force that would be needed to balance the system is 105 N. Therefore, the orbit that induces this restoration force into balance ring would be 4 mm.

We can also identify that the ring restoration force varies with either the rotation or eccentricity, even though the restoration water mass is more affected by the eccentricity.

In addition, Figure 7 presents the response surface of restoration force (N) as a function of rotation speed (rpm) and eccentricity (mm).

As a result of this study, it was possible to identify a steady state equation for the balance ring restoration mass and force which is based on rotation speed and orbit. This model might be described in

$$m = 0.0072 \cdot e \cdot (n)^{0.35},$$
$$\text{Fr} = 0.0072 \cdot e \cdot (n)^{0.35} \cdot \left(\frac{n \cdot 2 \cdot \pi}{60}\right)^2 \cdot r, \quad (1)$$

where m is the restoration mass (kg), e is the eccentricity (mm), n is the rotation speed (rpm), Fr is the restoration force of ring (N), and r is the ring radius (m).

In this table, we can also identify that the absolute ring force might not be affected by the orbit orientation, even though the translational component of motion results in different water distribution. In Figure 8, an illustration of balance ring water distribution that resulted from rotation of 500 rpm, 10 mm of eccentricity, and orbit orientation equal to 90° (a) and 180° (b) is presented.

In order to model the behaviour of balance ring in a computational way, we assumed that the balance ring has a local and movable coordinate system which is placed in the centre of the ring. As a consequence, the position of the local coordinate system at s-ésim time increment can be defined by

$$H_{\text{local}}(e) = \begin{bmatrix} \cos(\theta_{\text{global}}) & \sin(\theta_{\text{global}}) & x_{\text{global}} \\ -\sin(\theta_{\text{global}}) & \cos(\theta_{\text{global}}) & y_{\text{global}} \\ 0 & 0 & 1 \end{bmatrix} \cdot \begin{bmatrix} \cos(d\theta) & \sin(d\theta) & dx \\ -\sin(d\theta) & \cos(d\theta) & dy \\ 0 & 0 & 1 \end{bmatrix}^n, \quad (2)$$

where H_{local} is the position matrix of movable coordinate system in s-ésim time increment, s is the e-ésim time increment, x_{global} and y_{global} are the absolute distance between the centre ring and a fixed global coordinate system [m], θ_{global} is the absolute angle between the movable coordinate x-axis (ring) and a fix global coordinate system [rad], dx and dy are the decrement of movable coordinates in s-ésim time increment [m], and $d\theta$ is the decrement of angle in s-ésim time increment [rad].

At the same way, the rotation speed might be defined as

$$\omega = \frac{n}{60} \cdot 2 \cdot \pi = \frac{d\theta}{dt} = \frac{d}{dt} \begin{bmatrix} \cos(d\theta) & \sin(d\theta) & 0 \\ -\sin(d\theta) & \cos(d\theta) & 0 \\ 0 & 0 & 1 \end{bmatrix}, \quad (3)$$

where ω is the angular velocity [rad/s], n is the rotation speed [rpm], and $d\theta$ is the decrement of angle in an instant of time (dt) [rad].

Table 3: Results of steady state study.

Control factor			Response factors			
Rotation (rpm)	Eccentricity (mm)	Orbit orientation	Restoration force (N)	Restoration mass (kg)	Phase (deg)	Unbalance (300 g - ref)
50	1	0	0,15	0,022	180	1,65
50	4,5	0	0,7	0,102	180	1,65
50	8	0	1,4	0,204	180	1,65
50	11,5	0	2	0,292	180	1,65
50	15	0	2,65	0,387	180	1,65
225	1	0	6,5	0,047	180	33
225	4,5	0	37	0,267	180	33
225	8	0	65	0,468	180	33
225	11,5	0	85	0,612	180	33
225	15	0	100	0,721	180	33
400	1	0	20	0,046	180	105
400	4,5	0	125	0,285	180	105
400	8	0	230	0,524	180	105
400	11,5	0	295	0,673	180	105
400	15	0	340	0,775	180	105
575	1	0	50	0,055	180	217
575	4,5	0	280	0,309	180	217
575	8	0	480	0,530	180	217
575	11,5	0	660	0,728	180	217
575	15	0	800	0,883	180	217
750	1	0	105	0,068	180	370
750	4,5	0	500	0,324	180	370
750	8	0	1000	0,648	180	370
750	11,5	0	1300	0,843	180	370
750	15	0	1530	0,992	180	370
50	1	45	0,15	0,022	45	1,65
50	4,5	45	0,7	0,102	45	1,65
50	8	45	1,4	0,204	45	1,65
50	11,5	45	2	0,292	45	1,65
50	15	45	2,65	0,387	45	1,65
225	1	45	6,5	0,047	45	33
225	4,5	45	37	0,267	45	33
225	8	45	65	0,468	45	33
225	11,5	45	85	0,612	45	33
225	15	45	100	0,721	45	33
400	1	45	20	0,046	45	105
400	4,5	45	125	0,285	45	105
400	8	45	230	0,524	45	105
400	11,5	45	295	0,673	45	105
400	15	45	340	0,775	45	105
575	1	45	50	0,055	45	217
575	4,5	45	280	0,309	45	217
575	8	45	480	0,530	45	217
575	11,5	45	660	0,728	45	217
575	15	45	800	0,883	45	217
750	1	45	105	0,068	45	370
750	4,5	45	500	0,324	45	370
750	8	45	1000	0,648	45	370
750	11,5	45	1300	0,843	45	370
750	15	45	1530	0,992	45	370
50	1	90	0,15	0,022	90	1,65
50	4,5	90	0,7	0,102	90	1,65

Table 3: Continued.

Control factor			Response factors			
Rotation (rpm)	Eccentricity (mm)	Orbit orientation	Restoration force (N)	Restoration mass (kg)	Phase (deg)	Unbalance (300 g - ref)
50	8	90	1,4	0,204	90	1,65
50	11,5	90	2	0,292	90	1,65
50	15	90	2,65	0,387	90	1,65
225	1	90	6,5	0,047	90	33
225	4,5	90	37	0,267	90	33
225	8	90	65	0,468	90	33
225	11,5	90	85	0,612	90	33
225	15	90	100	0,721	90	33
400	1	90	20	0,046	90	105
400	4,5	90	125	0,285	90	105
400	8	90	230	0,524	90	105
400	11,5	90	295	0,673	90	105
400	15	90	340	0,775	90	105
575	1	90	50	0,055	90	217
575	4,5	90	280	0,309	90	217
575	8	90	480	0,530	90	217
575	11,5	90	660	0,728	90	217
575	15	90	800	0,883	90	217
750	1	90	105	0,068	90	370
750	4,5	90	500	0,324	90	370
750	8	90	1000	0,648	90	370
750	11,5	90	1300	0,843	90	370
750	15	90	1530	0,992	90	370

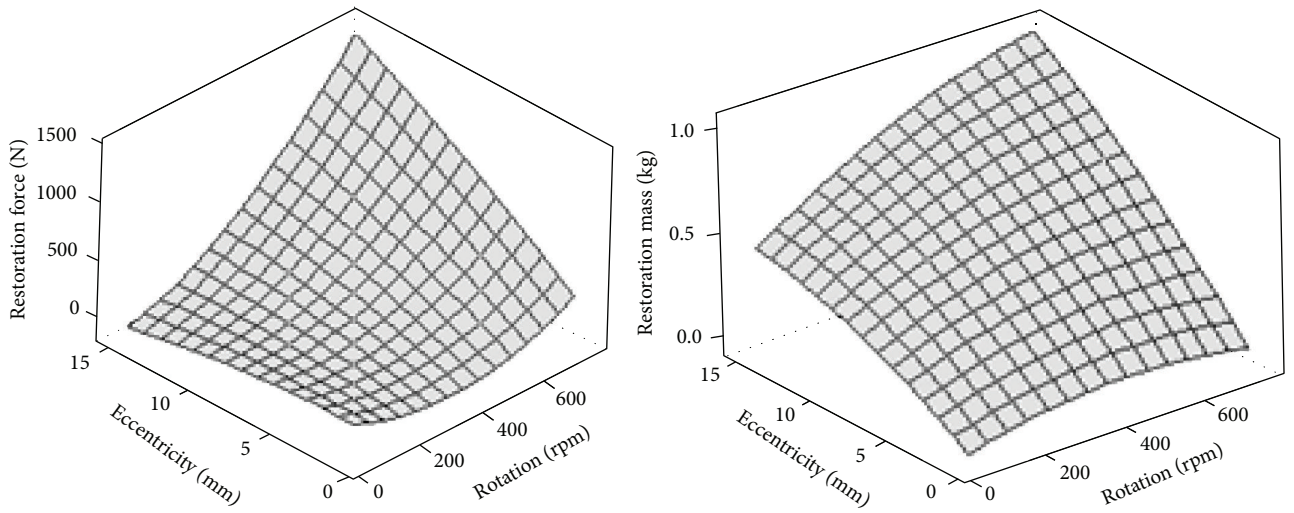

Figure 7: Response surface of steady state study correlating rotation speed (rpm), eccentricity (mm), restoration force (N), and restoration mass (kg).

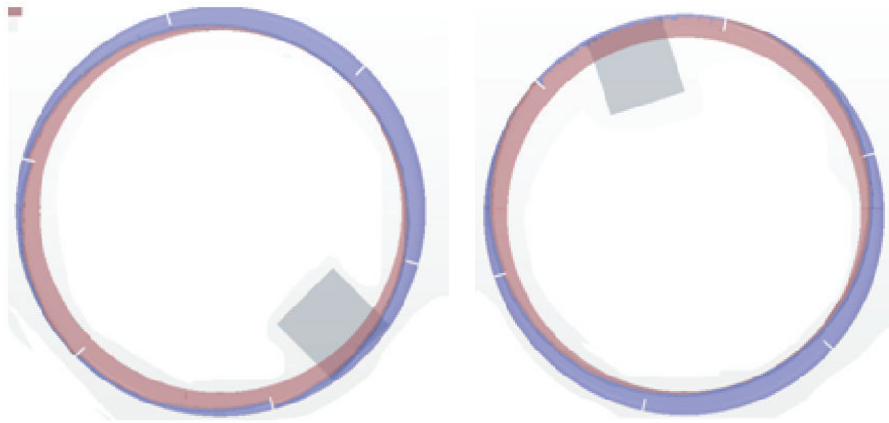

(a) (b)

Figure 8: Representation of balance ring water distribution for 10 mm eccentricity and 500 rpm rotation, where (a) is 90° phase angle and (b) is 180° phase angle.

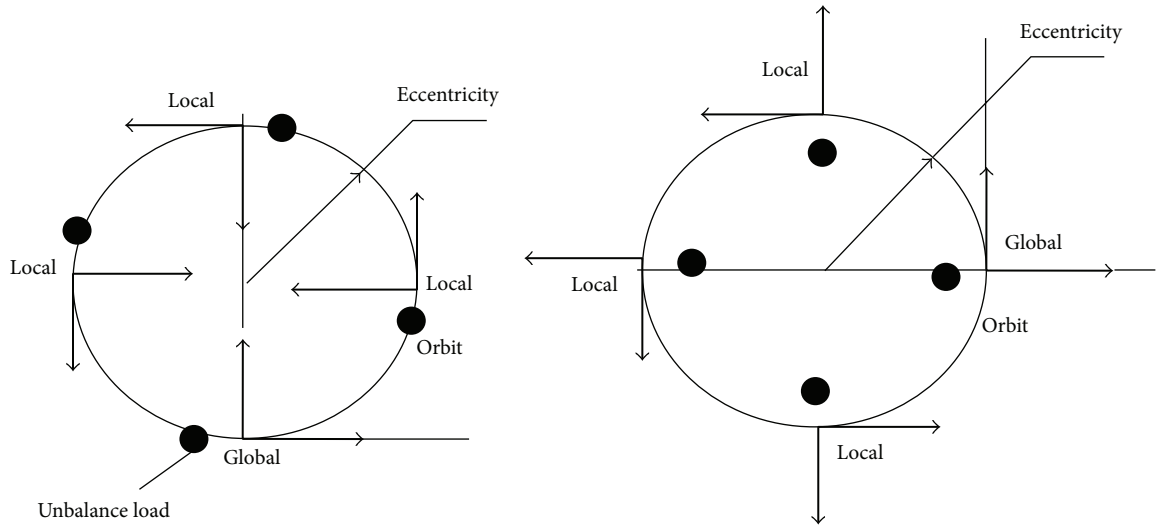

Figure 9: Schematic of orbit orientation for motion component: (a) angular velocity (ω), translational velocity in x-axis (v_x) and (b) angular velocity (ω), translational velocity in y-axis (v_y).

And, in consequence, the combination of translation and a constant rotation causes a defined eccentricity:

$$e = \frac{\sqrt{(dx/2)^2 + (dy/2)^2}}{\sin(d\theta/2)}. \tag{4}$$

Moreover, in spite of eccentricity, it is also possible to determine the orientation of movement with respect to the global coordinate and unbalance load, as presented in Figure 9.

It can be noted that each orbit orientation results in a different angle between the unbalance load which follows the local coordinate and the radial eccentricity vector. Therefore, we can define this orbit orientation angle (α) through

$$\alpha = a\cos\left(\frac{(dx/2)}{\sqrt{(dx/2)^2 + (dy/2)^2}}\right). \tag{5}$$

As a consequence, if we replace (3) and (4) into (1), we could find the absolute values of restoration mass (m) and restoration force (Fr):

$$m = 0.0072 \cdot \left(\frac{\sqrt{(dx/2)^2 + (dy/2)^2}}{\sin(d\theta/2)}\right) \cdot \left(\frac{d\theta}{dt} \cdot \frac{60}{2 \cdot \pi}\right)^{0.35},$$

$$\mathrm{Fr} = 0.0072 \cdot \left(\frac{\sqrt{(dx/2)^2 + (dy/2)^2}}{\sin(d\theta/2)} \right) \cdot \left(\frac{d\theta}{dt} \cdot \frac{60}{2 \cdot \pi} \right)^{0.35} \cdot \left(\frac{d\theta}{dt} \right)^2 \cdot r. \quad (6)$$

With respect to the transient study, it was possible to identify the transient equation for each change of state level, as presented in Table 2. In this table, it is possible to identify either transition time between steady states or transient equations. It is also important to highlight that these equations result from the same model, having just a small divergence in the coefficients values.

In spite of that, it might be noted that this transient equation is a function of time and, consequently, implied on a computational implementation in discrete time very hard. Therefore, we converted this equation from the time domain to the decrement of time domain in order to allow for doing the convolution operation.

The result of this conversion can be seen in (7) where the transient equation in time domain and decrement of time domain are presented, where m is the restoration mass as a function of time, m_c is the steady state restoration mass, and c is the transitional coefficient. In this equation, $d\tau$ is the increment of time or time step:

$$m_{(t)} = \int_0^t \left(m_{c(t)} - m_{c(t-\tau)} \right) \cdot c \cdot d\tau = \left(m_c - m_c \cdot e^{-c \cdot t} \right). \quad (7)$$

In addition, we can identify the increment of restoration mass at each instant of time according to (8), where dm is the increment restoration mass:

$$dm_{(t)} = \left(m_{c(t)} - m_{c(t-\tau)} \right) \cdot c \cdot d\tau. \quad (8)$$

Therefore, if we replace (6) into (7) we can find the transient model of LeBlanc stabilizer, where a is the angular model coefficient and δ is an exponential model coefficient:

$$m_{(t)} = m_{c(t-\tau)} + \left(a \cdot \frac{\sqrt{(dx/2)^2 + (dy/2)^2}}{\sin(d\theta/2)} \cdot \left(\frac{60}{2 \cdot \pi} \cdot \frac{d\theta}{d\tau} \right)^{\delta} - m_{c(t-\tau)} \right) \cdot c \cdot d\tau,$$

$$\mathrm{Fr} = \left(m_{c(t-\tau)} + \left(a \cdot \frac{\sqrt{(dx/2)^2 + (dy/2)^2}}{\sin(d\theta/2)} \cdot \left(\frac{60}{2 \cdot \pi} \cdot \frac{d\theta}{d\tau} \right)^{\delta} - m_{c(t-\tau)} \right) \cdot c \cdot d\tau \right) \cdot \left(\frac{d\theta}{dt} \right)^2 \cdot r. \quad (9)$$

Therefore, this model might indicate the instantaneous values of restoration force (Fr), equivalent unbalance mass (m), and phase angle between unbalance load and restoration force as a function of ring translational decrement (dx, dy) and ring angular decrement ($d\theta$).

At the end, we applied this numerical model into a rigid body model with 3 degrees of freedom (DoF), identifying the force of unbalance load, restoration force, orbit, and phase angle between unbalance load and restoration force.

In Figure 10, the results of dynamic system with no balance ring analyses are presented, where the diagrams of orbit displacement and unbalance load represent the main responses of this study.

In this figure, it is possible to see that, at the final stage, the orbits tend to increase as a function of rotation acceleration, while the initial stages of analyses are marked by a pick of orbit, which might be related to the natural frequency of system. In either cases, we can also identify that unbalance load is implied on a force between 950 and 1000 N, resulting in additional stress and deflection of mechanical components, such as basket, hub, and shaft. For example, if we considered that the basket height is 500 mm and the unbalance load is placed at the middle height, the moment at the tip of motor shaft would be approximately 250 N·m. Moreover, this effort might be implied on excessive deflection of basket (interference between tub and basket) or even the collapse of system.

On the other hand, Figure 11 shows the dynamic systems analyses which considered balance ring. It is possible to see that the balance ring causes a reduction of orbit at intermediate and final stages, even though the initial stages still present the pick of orbit which is related to natural frequency. Otherwise, for that configuration of dynamic system, the values of orbit eccentricity have been shown to be reduced from 10 to 6 mm, indicating a tremendous improvement from the vibration perspective.

In spite of that, it is important to note that the balance ring resulted in forces from 750 to 850 N at the final stages. Therefore, if we considered basket with height equal to 500 m, the unbalance load at the middle height and the balance ring that the top of basket, the resulting moment at the tip of motor shaft would be 125 N·m. That moment decreasing (125 N·m) might result, for example, in the decrease of shaft diameter and consequently the decrease of cost. On the other hand, this condition makes also it possible to increase rotation and washing machine capacity.

At the end, it was possible to see that the contribution of LeBlanc stabilizer for the washing machine dynamics is extremely important, whereas it reduces the obit of system in transient state and reduces efforts in structural mechanical components, such as basket and shaft.

4. Conclusions

In conclusion, both new steady and transient state models were proposed in this work, being possible to characterize the general behaviour of LeBlanc stabilizer as a function of rotation speed, eccentricity, and orbit orientation.

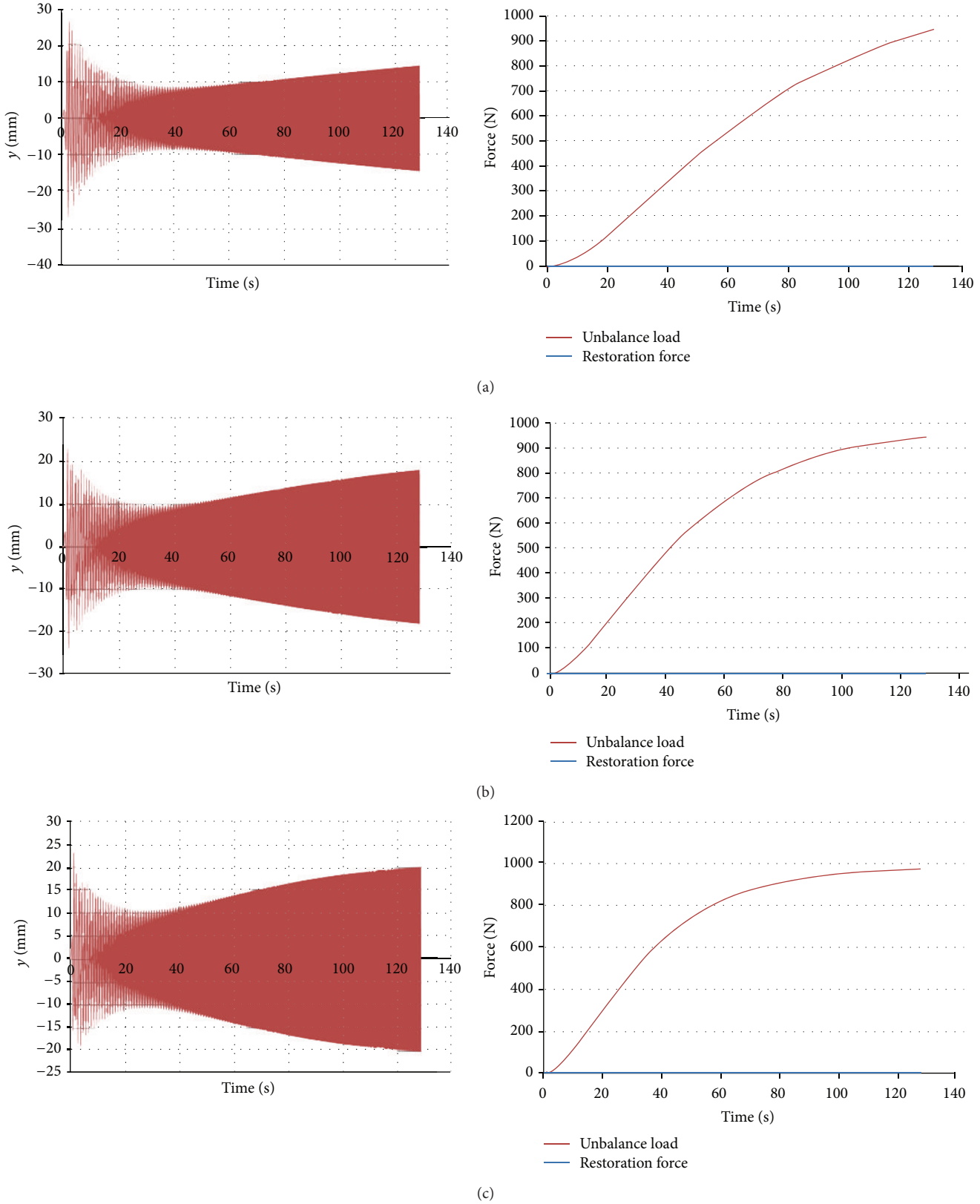

Figure 10: Diagram of orbit displacement (y direction) and unbalance load for system without balance ring with ramp acceleration equal to (a) 15 rpm/s; (b) 20 rpm/s; and (c) 25 rpm/s.

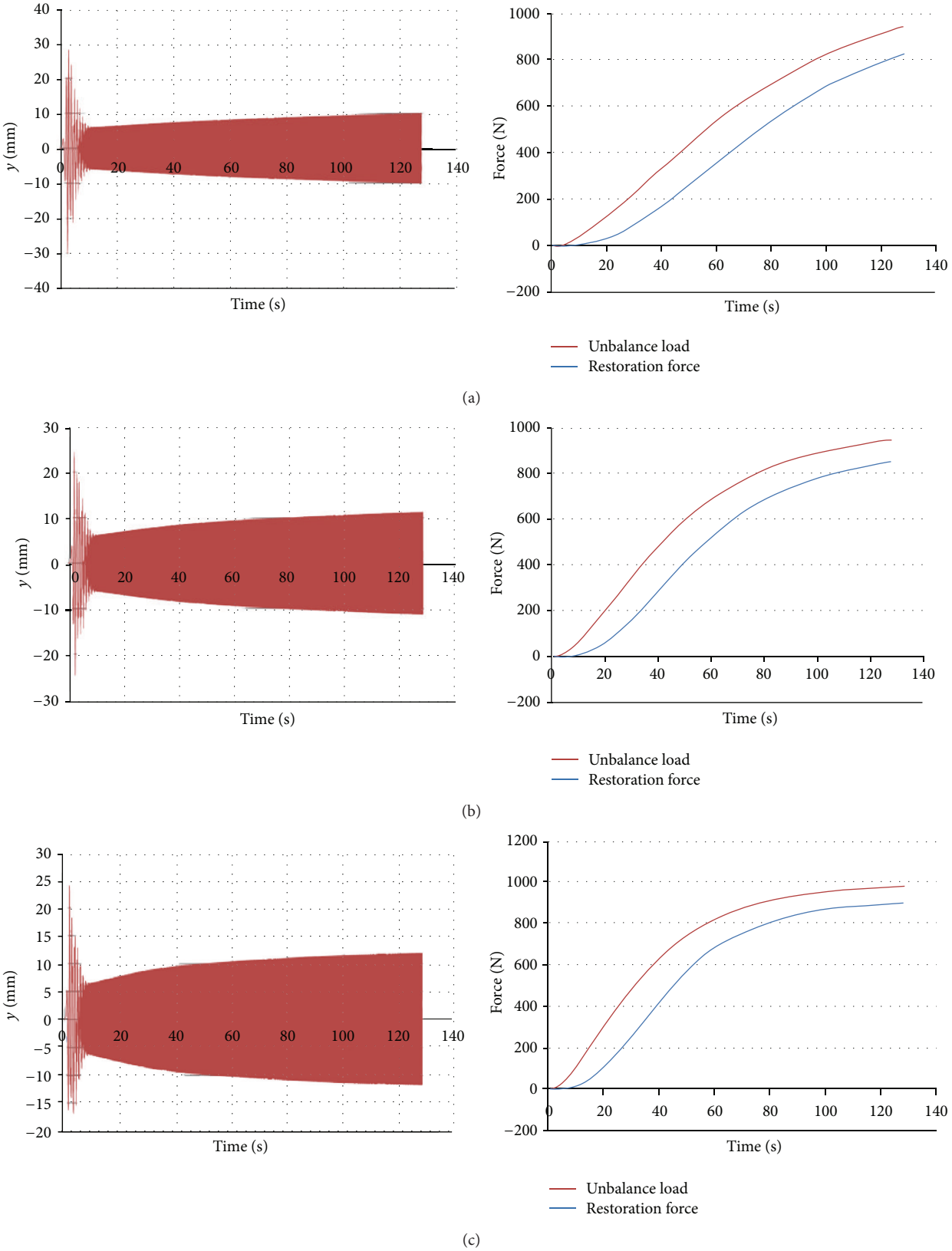

Figure 11: Diagram of orbit displacement (y direction) and unbalance load for system with balance ring with ramp acceleration equal to (a) 15 rpm/s; (b) 20 rpm/s; and (c) 25 rpm/s.

In this work, it was also possible to find a simplified equation of restoration mass and force, as well as the phase angle between this force and the reference unbalance load. In addition, a model which is based on 3 degrees of freedom motion was also proposed, where the rotation, eccentricity, and orbit orientation could be described through the rotational and translational increments at time ($d\theta$, dx, and dy).

On the other hand, this work also allows for finding transient equations which are based on time and increment of time domains. Therefore, for the characterization of balance ring, the time domain model helps us to compare efficiency of balance rings in an easy way (transition time between states), while the increment of time model does to implement the model computationally.

As a result of this model, we have been able to build a simplified dynamic model with 3 DOF, where it was possible to identify the general behaviour of a balance ring in a dynamic system besides predicting the response of this system.

On the other hand, it can be helpful to other sorts of analyses, such as the prediction of basket deflection through the difference between unbalance and restoration forces.

Moreover, in spite of the fact that this work still has several challenges to be overcome, this work presented a novel approach for the characterization of LeBlanc stabilizer which make it possible to represent balance rings behaviour in dynamics simulation without computational performance drawbacks.

Conflict of Interests

The author declares that there is no conflict of interests regarding the publication of this paper.

References

[1] A. Thompson-Salinas, M. Ortega-Breña, M. H. de la Torre-Ibarra, B. Barrientos-García, and V. J. Gonzalez-Villela, "Hydraulic balance ring study and design using optical techniques," in *Proceedings of the ASME International Mechanical Engineering Congress and Exposition*, pp. 371–381, Denver, Colo, USA, November 2011.

[2] H. S. Hoon, L. J. Young, S. Suzuki, and H. W. Gu, "A study on the dynamic behaviour of an automatic washing machine," *Nippon Kikai Gakkai Kankyo Kogaku Sogo Shinpojiumu Koen Ronbunshu*, vol. 11, pp. 131–134, 2001.

[3] H.-W. Chen, W.-X. Ji, Q.-J. Zhang, Y. Cao, and S.-Y. Fan, "A method for vibration isolation of a vertical axis automatic washing machine with a hydraulic balancer," *Journal of Mechanical Science and Technology*, vol. 26, no. 2, pp. 335–343, 2012.

[4] H.-W. Chen and Q.-J. Zhang, "Stability analyses of a vertical axis automatic washing machine without balancer," *Journal of Sound and Vibration*, vol. 329, no. 11, pp. 2177–2192, 2010.

[5] H.-W. Chen and Q.-J. Zhang, "Stability analyses of a vertical axis automatic washing machine with a hydraulic balancer," *Mechanism and Machine Theory*, vol. 46, no. 7, pp. 910–926, 2011.

[6] H.-W. Chen, Q.-J. Zhang, and S.-Y. Fan, "Study on steady-state response of a vertical axis automatic washing machine with a hydraulic balancer using a new approach and a method for getting a smaller deflection angle," *Journal of Sound and Vibration*, vol. 330, no. 9, pp. 2017–2030, 2011.

[7] C.-H. Jung, C.-S. Kim, and Y.-H. Choi, "A dynamic model and numerical study on the liquid balancer used in an automatic washing machine," *Journal of Mechanical Science and Technology*, vol. 22, no. 9, pp. 1843–1852, 2008.

[8] V. Royzman and I. Drach, "Improving theory for automatic balancing of rotating rotors with liquid self balancers," *Mechanika*, vol. 4, no. 54, pp. 38–43, 2005.